Treatment head disassembly to improve the accuracy of large electron field simulation

Bruce A. Faddegon,[a] Daren Sawkey, and Tuathan O'Shea
Department of Radiation Oncology, UC San Francisco (UCSF) Comprehensive Cancer Center, San Francisco, California 94143-1708

Malcolm McEwen and Carl Ross
Ionizing Radiation Standards, Institute for National Measurement Standards, National Research Council, Ottawa, Ontario K1A 0R6, Canada

(Received 19 February 2009; revised 7 August 2009; accepted for publication 11 August 2009; published 11 September 2009)

Purpose: The purposes of this study are to improve the accuracy of source and geometry parameters used in the simulation of large electron fields from a clinical linear accelerator and to evaluate improvement in the accuracy of the calculated dose distributions.
Methods: The monitor chamber and scattering foils of a clinical machine not in clinical service were removed for direct measurement of component geometry. Dose distributions were measured at various stages of reassembly, reducing the number of geometry variables in the simulation. The measured spot position and beam angle were found to vary with the beam energy. A magnetic field from the bending magnet was found between the exit window and the secondary collimators of sufficient strength to deflect electrons 1 cm off the beam axis at 100 cm from the exit window. The exit window was 0.05 cm thicker than manufacturer's specification, with over half of the increased thickness due to water pressure in the channel used to cool the window. Dose distributions were calculated with Monte Carlo simulation of the treatment head and water phantom using EGSnrc, a code benchmarked at radiotherapy energies for electron scatter and bremsstrahlung production, both critical to the simulation. The secondary scattering foil and monitor chamber offset from the collimator rotation axis were allowed to vary with the beam energy in the simulation to accommodate the deflection of the beam by the magnetic field, which was not simulated.
Results: The energy varied linearly with bending magnet current to within 1.4% from 6.7 to 19.6 MeV, the bending magnet beginning to saturate at the highest beam energy. The range in secondary foil offset used to account for the magnetic field was 0.09 cm crossplane and 0.15 cm inplane, the range in monitor chamber offset was 0.14 cm crossplane and 0.07 cm inplane. A 1.5%/0.09 cm match or better was obtained to measured depth dose curves. Profiles measured at the depth of maximum dose matched the simulated profiles to 2.6% or better at doses of 80% or more of the dose on the central axis. The profiles along the direction of MLC motion agreed to within 0.16 cm at the edge of the field. There remained a mismatch for the lower beam energies at the edge of the profile that ran parallel to the direction of jaw motion of up to 1.4 cm for the 6 MeV beam, attributed to the MLC support block at the periphery of the field left out of the simulation and to beam deflection by the magnetic field. The possibility of using these results to perform accurate simulation without disassembly is discussed. Phase-space files were made available for benchmarking beam models and other purposes.
Conclusions: The match to measured large field dose distributions from clinical electron beams with Monte Carlo simulation was improved with more accurate source details and geometry details closer to manufacturer's specification than previously achieved. [DOI: 10.1118/1.3218764]

Key words: Monte Carlo, beam model, electron therapy, treatment head simulation

I. INTRODUCTION

Electrons are widely used in radiotherapy to take advantage of the steep falloff of dose with depth, reducing the energy imparted to healthy tissue. Improvements in electron dose delivery through automated aperture setting with a multileaf collimator (MLC) are anticipated, either one specifically designed for modulated electron radiotherapy or by the x-ray MLC already installed on the linear accelerator (linac).[1,2] Such technical advances demand high accuracy in the calculation of fluence and dose. The high accuracy and detail of the Monte Carlo method of simulating trajectories of individual particles through complex geometries have proven valuable for this purpose, with Monte Carlo simulation now offered in some commercial treatment planning systems.[3]

A benchmark of clinical electron beam fluence with 2% accuracy or better would be valuable for validating beam models used in these systems. A recent benchmark of electron scatter is available with this accuracy.[4] This benchmark

is limited to scatter from single foils. The treatment head of a clinical linac is outfitted with a more complicated set of components; therefore, a clinical fluence benchmark is best determined on a clinical machine.

The Monte Carlo method provides one of the most accurate means of calculating fluence from a detailed treatment head simulation (see Refs. 5 and 3 and papers on treatment head simulation referenced therein). The method can theoretically achieve the 1%–2% accuracy sought, should the underlying radiation transport methodology and interaction data be sufficiently accurate, as well as the specific implementation of the code. The electron source and treatment head geometry must be fully and accurately specified. Published results for a Siemens linac show simulation is capable of achieving a 2%–4% match to measured dose distributions in the central region of the largest available electron field, reduced accuracy in the field edge, with a reasonable match to the shape of the profile in the bremsstrahlung region.[6] The agreement was achieved with the focal spot position and beam angle set the same for all beam energies, an incorrect assumption as shown below, and the exit window thickness and secondary foil thickness adjusted outside the manufacturer's specification. A similar match was achieved for the largest electron field of a Varian linac.[7] The source was modeled with an unusually broad angular distribution produced with a normally incident beam using an unusually large spot size at the primary scattering foil. More accurate simulations are needed.

This paper presents methodology to improve the accuracy of Monte Carlo treatment head simulation for large electron fields, including methods that require partial disassembly of the treatment head that may be impractical in a clinical setting. The linac was a Siemens Oncor (Siemens Oncology Care Systems, Concord, USA). Simulation took advantage of the EGSnrc Monte Carlo system, recently validated with a thick-target bremsstrahlung experimental benchmark available for radiotherapy energy beams[8] and an electron scatter benchmark for clinical beam energies and scattering foils.[4] Measurement took advantage of a clinical machine that was not in clinical service, allowing the components of the treatment head to be removed, and giving time to take careful measurements with many repeats. The treatment head was disassembled for direct measurement of components and to set a tight tolerance on specific source and geometry values used in the simulation. Dose distributions were measured at various stages of reassembly to characterize the electron source with minimal material in the beam path and to reduce the number of geometry variables at each stage of the simulation, with the intent of improving the accuracy of these variables.

II. MATERIALS AND METHODS

II.A. Water tank scans

The measurements used in the adjustment of simulation source and geometry details were made starting with the treatment head configuration with no scattering foils in place and the monitor chamber removed (no foil configuration in Fig. 1). Next, the primary foil was added (primary foil configuration), and finally both scattering foils and the monitor chamber were placed back in the treatment head (clinical configuration). Primary foil selection, including the selection of no primary foil, was easily done from the linac console. These measurements were taken over a 4 month period, with tight control on equipment setup and beam tuning, showing reproducibility within experimental uncertainty. Dose distributions measured at each stage of reassembly were compared to Monte Carlo simulation. Measurements done prior to disassembly were not used for this purpose. This eliminated uncertainty due to differences in component position (foil and chamber) prior to disassembly and following reassembly.

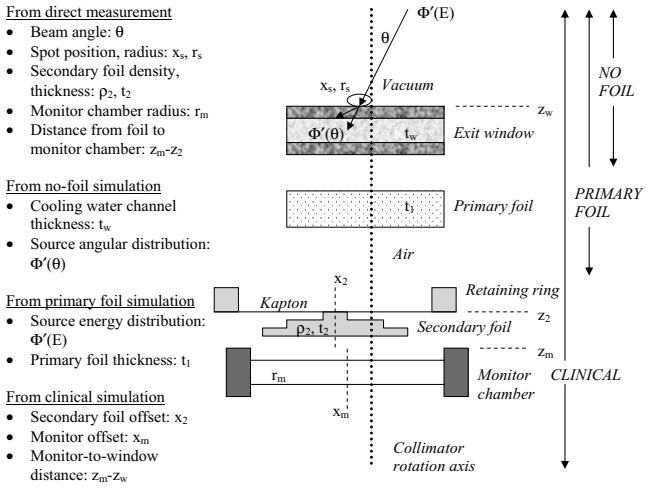

FIG. 1. Treatment head from exit window to monitor chamber (not to scale). The source and geometry parameters shown were either measured directly or adjusted iteratively in the simulation to match measured dose distributions for the different treatment head configurations: no foil, primary foil, and clinical. Not all parameters are shown.

Beam tuning and dose calibration were done through a set of soft pots adjusted from the linac console. Adjustments available included accelerating potential, beam energy selection (bending magnet current), pulse rate, spot position (steering current), and beam current. The tuning was kept the same for the different treatment head configurations.

Central axis percentage depth ionization (PDI) curves, percentage depth dose (PDD) curves, and horizontal dose profiles in the inplane (IP) and crossplane (CP) directions were measured in water in a $60\times63\times58$ cm^3 scanning water tank (IBA Dosimetry Bartlett, TN) with improvement in the method used in the previous study,[9] following accepted commissioning procedure.[10] The inplane direction was positive toward the gun, the crossplane direction positive to the right when facing the gantry. The source-surface distance (SSD) was 100 cm and, unless otherwise stated, the secondary collimators were fully open and no applicator was present. Repeat scans were averaged to improve the experimental uncertainty. PDI were shifted to the average I_{50} of the measurements before averaging to maintain the slope of the fall-off portion of the curve.

Gantry and collimator angles were set to 0.1°. Jaw and MLC position repeatability was 0.1 cm, projected to the iso-

TABLE I. Characteristics of measured (mst) and simulated (sim) PDI and PDD. Depth of 50% ionization in PDI, I_{50}, measured with a parallel-plate chamber. Depth of 50% dose in PDD, R_{50}, measured with a diode. The nominal depth of maximum dose, R_{max}. Depth of measurement in bremsstrahlung region 2–3 cm beyond practical range, R_x.

			Nominal beam energy (MeV)					
Configuration	Parameter	Method	6	9	12	15	18	21
No foil	I_{50} (cm)	mst	2.50	3.80	4.95	6.37	7.75	8.47
		sim	2.51	3.80	4.93	6.38	7.76	8.47
Primary foil	I_{50} (cm)	mst	–	3.71	4.88	6.18	7.61	8.43
		sim	–	3.72	4.88	6.19	7.61	8.46
Clinical	I_{50} (cm)	mst	2.31	3.52	4.68	5.98	7.41	8.24
		sim	2.40	3.60	4.74	6.06	7.47	8.30
Clinical	R_{50} (cm)	mst	2.37	3.61	4.77	6.10	7.61	8.47
		sim	2.42	3.63	4.80	6.14	7.63	8.50
Clinical	R_{max} (cm)	mst	1.3	2.0	2.7	3.0	2.1	1.9
Clinical	R_x (cm)	mst	5.0	7.0	8.0	10.0	12.0	13.0

center. The relative position of the detector was known to be 0.04 cm, and there was a minimal backlash. The detector carriage was set parallel to the water surface to within 0.1 cm over the full length of carriage travel. There was a 0.1 cm downward bow at the center of the carriage motion crossplane.

The scan origin was set at the mechanical isocenter of the linac. The water surface was positioned to within 0.1 cm of the isocenter. The detector was centered to within 0.03 cm of the collimator rotation axis, matching the 0° collimator and mirrored 180° collimator crossplane and inplane profile field edges measured at the depth of maximum dose R_{max} for the 12 MeV beam collimated with one of the square applicators (usually 10×10 cm^2).

II.A.1. Horizontal dose profiles

Horizontal profiles were measured with a CC13 ion chamber (IBA Dosimetry) at R_{max}. Profiles were also measured in the bremsstrahlung tail at the depth R_x, previously R_{p+},[9] 2–3 cm beyond the practical range (Table I). This is just deep enough to avoid including dose from primary electrons in the rebinned volume of the calculated dose distribution, used to give reasonable statistical precision. The axis of the chamber was oriented inplane. The chamber was positioned to place the effective point of measurement of 0.15 cm (half of the chamber radius)[10] to within 0.1 cm of the water surface. With the dose normalized to 100% at the profile peak, the uncertainty in profiles was 0.5%/0.05 cm (1 standard deviation).

The CC13 was preferred over diodes used previously,[9] which exhibited noisier scans and a significant error due to over-response to x rays. Profiles measured with the CC13 were compared to those measured with an N60008 diode (PTW, Freiburg, Germany) and an EFD diode (IBA Dosimetry). The off-axis ratio measured with the CC13 was 1.2% higher at 12–14 cm off axis for 18–21 MeV than that measured with these diodes, the field width at 50% of the central axis 0.06–0.46 cm larger, increasing with energy. The effect increases with energy due to the increased bremsstrahlung. The dose rate and directional dependence of the diodes were measured and found to contribute negligibly to the discrepancy. Diode over-response to x rays was shown to be the source of the discrepancy as follows. The x-ray component at R_{max}, calculated with Monte Carlo simulation, was multiplied by the measured over-response of the diodes in the bremsstrahlung tail of the PDD and the result subtracted from the R_{max} diode profiles. The corrected diode profiles were within 0.5% of the off-axis ratios and 0.14 cm of the field widths measured with the CC13. The CC13 scans were used exclusively in simulation parameter tuning.

II.A.2. Depth penetration

PDI was measured with two different parallel-plate chambers: A Roos chamber (PTW N34001) and an NACP chamber (NACP 75-10). The effective point of measurement was 0.115 cm for the Roos chamber and 0.100 cm for the NACP chamber, based on the manufacturer's specification of wall thickness and density and ICRU values for the stopping power of the wall.[11] PDDs were measured with EFD and PTW diodes with effective point of measurement of 0.045 and 0.065 cm, respectively. To compare parallel-plate and diode measurements, the PDI curves were converted to dose to water using the water-to-air stopping power ratio calculated using standard methods,[12] as part of the Monte Carlo simulation in the water phantom.

In the no foil configuration, the detector was offset from the collimator rotation axis at the position of the peak in the horizontal profiles. This was important for the higher energy beams where the profile was narrow enough for the depth of 50% dose, R_{50}, to be affected by the offset. The deepest point of the scan was used as the start point, time was given for water ripples to die down, and a constant scan speed was used, slow enough to prevent the water surface from bulging upward when the detector approaches the surface.

The accuracy of positioning the detectors relative to the water surface was estimated with a water tank from the National Research Council of Canada (NRCC). The uncertainty

TABLE II. Treatment head details used in the simulation compared to manufacturer specification. In the Method column, "Check" means specification checked with direct measurement, "Sim A" means values determined through simulation of the no foil configuration, Sim B means the primary foil configuration, and Sim C means the clinical configuration. Primary foil thickness adjustment shown in both relative and absolute values. Offsets are relative to the collimator rotation axis, both CP and IP. Secondary collimator positions specified at the collimator surface closest to the exit window.

		Nominal beam energy (MeV)					
Parameter	Method	6	9	12	15	18	21
Primary foil thickness	Sim B	–	−6%	−8%	−3%	−5%	−5%
Primary foil thickness	Sim B (μm)	–	8	4	4	9	10
Secondary foil offset CP	Sim C (cm)	−0.07	−0.05	−0.01	0	0	0.02
Secondary foil offset IP	Sim C (cm)	−0.08	−0.03	0.01	0.01	0.02	0.07
Chamber offset CP	Sim C (cm)	−0.11	−0.04	−0.025	0.02	0.02	0.03
Chamber offset IP	Sim C (cm)	−0.21	−0.17	−0.15	−0.14	−0.14	−0.17
Exit window	Sim A	0.05 cm thicker water channel					
Secondary foil geometry	Check	No change in thickness ±0.0001 cm, inner ring diameters ±0.03 cm, outer ring diameter ±0.003 cm					
Secondary foil density	Check	No change ±1.5%.					
Secondary foil retaining ring diameter	Check	No change ±0.003 cm					
Secondary foil retaining ring thickness	Check	Thicker by 0.147 cm					
Kapton holding secondary foil	Check	Thinner by 0.005 ± 0.001 cm					
Window to chamber distance	Sim C	Increased 0.12 cm					
Chamber diameter	Check	No change ±0.003 cm					
Chamber to isocenter distance	Check	Closer by 0.3 ± 0.1 cm					
CP MLC position at 27.75 cm	Sim B (cm)	0, 0.02 (MLC opening of −5.55, 5.57)					
IP jaw position at 19.89 cm	Sim B (cm)	0.02, 0.02 (Jaw opening of −4.01, 3.96)					

in detector position was 0.01 cm largely due to the slight pressure on the Mylar wall from the machined brass rod used to calibrate the position. The depth of 50% ionization, I_{50}, and depth of 50% dose, R_{50}, measured in the IBA water tank (vertical beam) was within 0.03 cm of that measured in the NRCC water tank (horizontal beam) for the 6 beam energies for the Roos chamber and the PTW and EFD diodes.

The uncertainty in depth penetration for the diode was 0.04 cm, 0.03 cm for chamber position relative to the water surface, and 0.03 cm for water evaporation and ripples. The I_{50} measured by the NACP chamber shifts 0.06 cm deeper after applying a published correction factor.[13] The uncertainty for the Roos chamber of 0.07 cm includes a 0.06 cm uncertainty for a possible depth-dependent change in electron perturbation factors since the PDI curves measured with the NACP and Roos chambers in the NRCC water tank agreed to 0.5%/0.02 cm. Measurements done on the same day with different chambers (Roos, EFD, and PTW), repeated on a number of occasions over the course of several years, were consistent with the uncertainty estimate.

The diode over-response to x rays had minimal effect on the PDD from the surface to R_{50}. The diode over-response had a much greater effect on the profiles of the high-energy beams due to the much larger drop in bremsstrahlung over the width of the profile than the length of the PDD. The effect on the 21 MeV PDD, with the largest bremsstrahlung component, was a 0.6% overestimate of the surface dose and a 0.02 cm increase in R_{50}. This was determined by subtracting the calculated bremsstrahlung component of the depth dose curve multiplied by the measured diode over-response in the bremsstrahlung tail, as done for the profiles.

II.B. Direct measurement of source and geometry details

II.B.1. Treatment head component geometry

Siemens has provided specifications for the geometry and material of treatment head components on a standard spreadsheet for Monte Carlo simulation. Adjustments were made to the specifications of a few components to improve the match between simulated and measured dose distributions, with full justification (see Sec. II E). For the most part, the specification from the spreadsheet was used, with standard material compositions and densities. The exit window was shifted 0.229 cm toward the isocenter, based on additional information provided by the manufacturer. This shift reduces the off-axis ratio in the clinical configuration by 0.5%, as shown with simulation.

The geometry, density, and relative positions of key components specified by the manufacturer were checked with direct measurement. These components are listed in Table II, identified as the "Check" method. A spare secondary foil with holder was taken apart to measure the foil geometry and density and the thickness of the plastic sheet (Kapton) and retaining rings used to hold the foil in place.

II.B.2. Spot size and position

The linac used in this study had 6 and 18 MV x-ray beams. The spot size of these beams was measured in the crossplane and inplane directions with a spot size camera and found to be from 0.12–0.21 cm in diameter full width at half maximum (FWHM). This was close to the spot size on the exit window for the electron beams. The spot size did not

need to be determined more accurately as the dose distribution of the large field was insensitive to spot size.[14]

The position of the spot was measured relative to the collimator rotation axis to within 0.03 cm using the following procedure. The thickest high-Z primary foil, normally used to scatter the 18 and 21 MeV electron beams, was put in the beam path for all of the beams. This foil produced more bremsstrahlung per incident electron and a flatter x-ray beam than the other foils. The field size was set to 5×5 cm^2. The opposing jaw and MLC leaves were first set to the same distance from the collimator rotation axis by comparing the 18 MeV beam R_x crossplane and inplane profiles scanned at 0° and 180° collimator setting. The offset of the spot from the collimator rotation axis at the primary foil was then obtained for each energy beam from the crossplane and inplane scans at R_x with the collimator at 0° and 90°. With the peak in each profile normalized to 100%, the shift on each side of the collimator rotation axis was the difference in the absolute value of the position of the 50% dose points on the profiles measured at the two collimator angles. With the paired collimators positioned the same distance from the collimator rotation axis, similar triangles may be used to show the spot position, x_s, is related to the difference in the shift on either side of the axis, Δ, by,

$$x_s = 59\Delta/(R_x + \mathrm{SSD}). \quad (1)$$

The factor of 59 was determined from the distance from the primary scattering foil to the downstream surface of the jaw s_{jaw} of 27.5 cm, and to the downstream surface of the MLC s_{MLC} of 35.8 cm, as the reciprocal of

$$2(1/s_{\mathrm{jaw}} - 1/s_{\mathrm{MLC}}). \quad (2)$$

Two sets of measurements done several months apart were used to determine the spot position and confirm the uncertainty. In these measurements, the central MLC leaves were set the same distance from the collimator rotation axis to within 0.01 cm, measured at R_x, the paired jaws to within 0.02 cm.

II.B.3. Beam angle

With the primary scattering foil in place, the beam at the foil is directed toward the peak in the R_x profile, as the dose at this depth is dominated by bremsstrahlung from the foil. The peak position was determined by fitting a Gaussian distribution to the profile in the region to within 10 cm of the collimator rotation axis, avoiding the decidedly non-Gaussian shape outside this region.

The 6 MeV clinical beam had no primary scattering foil. In this case, the proportion of dose at the peak in the R_x profile from photons originating in the treatment head, primarily from the exit window and secondary scattering foil, was 48% of the total dose calculated using Monte Carlo simulation. Since the bremsstrahlung from the water had a nearly flat profile, the beam angle could still be determined from the position of the peak in the R_x profile. The beam angle used in the 6 MeV clinical beam simulation was determined from the peak in the simulated R_x profile to within 0.1°, supporting this contention.

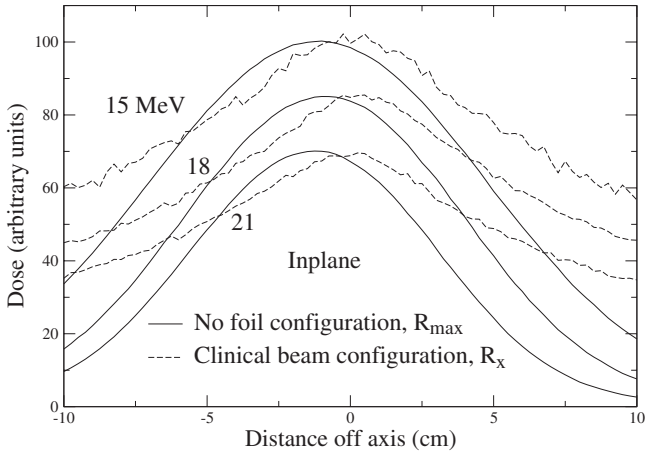

FIG. 2. Profiles measured at R_{max} in the no foil configuration (solid lines) compared to profiles measured in the bremsstrahlung tail at R_x for the clinical beams. The relative shift in the peaks in the electron and bremsstrahlung profiles is due to the presence of a magnetic field between the exit window and the monitor chamber.

II.C. Magnetic field

Inplane profiles measured in the no foil configuration at R_{max} and the clinical configuration at R_x for the 15–18 MeV beams are shown in Fig. 2. There is a distinct difference in the position of the peaks in the profiles. The shift is due to the presence of a magnetic field in the region between the exit window and secondary scattering foil which defects the electron beam away from the axis of the x-ray beam generated in the exit window and primary foil. The field, measured with a gaussmeter (F.W. Bell model 4048, Syprus, Orlando, FL), was highly inhomogeneous. The highest intensity on the collimator rotation axis was at the exit window. The intensity at this point increased with the bending magnet current (beam energy) from 0.004 to 0.012 T, demonstrating the source of the magnetic field was the bending magnet. The magnetic field was oriented approximately in the crossplane direction, deflecting electrons inplane. The field intensity measured was sufficient to deflect the electron beams by the amount observed.

The magnetic field was "discovered" well into this work and it was decided to continue simulation without it for several reasons. To our knowledge, the magnetic field has not been explicitly modeled in the past and may not even have been observed. The refined procedures and the measurements done with the secondary foil and monitor chamber removed resulted in a much better match to measurement than previously published and this with more highly constrained source and geometry parameters. It would help those wishing to simulate their own linac to know the accuracy achieved without mapping the magnetic field, a difficult measurement for clinical machines, and requiring the removal of the secondary foil and monitor chamber.

II.D. Monte Carlo simulation

The user code BEAMnrc (Ref. 15) (version 1.104, July 24, 2008) was used with the Monte Carlo system EGSnrc (Ref. 16) (version 1.40, July 24, 2008) to simulate the treatment head. The code was also modified to allow a crossplane and inplane shifts of each component module.[8] Source 19, a point source with Gaussian focal spot, was modified to permit a Gaussian angular distribution with arbitrary beam direction. The phase space was scored on a plane 10 cm above the linac isocenter and these particles tracked with the user code MCRTP (Ref. 17) through a 50 cm wide cube of water at 100 cm SSD. Transport parameters were the same as used in a recent publication[6] except that bremsstrahlung cross sections from NIST were used. The differences in the choice of photon transport parameters from the recently published comparison of EGSnrc to experimental benchmarks[4] are reasonable and did not significantly affect the results.

There were 100 million source electrons followed in the no foil configuration for the 6 MeV beam, 50 million for the 9–21 MeV beams. There were 100 million electrons in the primary foil configuration, and 800 million in the clinical configuration. A network of Dell T5400n computers with a total of 32 2 GHz processors was used to keep the simulation time for a full set of 6 beams in the clinical configuration down to 2–3 days.

Both dose to water and dose to a Bragg–Gray cavity of air, calculated using standard methods,[12] were scored in the water phantom in 0.25 cm wide, 0.1 cm deep voxels. Simulated dose distributions were averaged over adjacent voxels (rebinned) in the directions orthogonal to the plotted data to improve the precision of the calculated profiles and PDDs while having minimal effect on the plotted quantity: 0.5×0.5 cm^2 for the no foil configuration and 1×1 cm^2 for the primary foil and clinical configurations. The R_{max} profile bin was 1×0.5 cm^2 deep for the no foil configuration, 2×0.5 cm^2 deep for the primary foil and clinical configurations. The R_x profile bin was 2×2 cm^2 deep. The precision roughly scaled with the square root of the increased area perpendicular to the beam direction in the electron region, the square root of the volume in the bremsstrahlung region. This led to a dose calculation precision of D_{max} (dose at R_{max}) of 0.3% or better for all treatment head configurations and a precision in the calculation of D_x (dose at R_x) of 0.8% at 6 MeV, reducing to 0.3% at 15–21 MeV.

Different detectors were chosen for different measurements such that volume averaging had negligible effect on the results. The measurements were averaged over the same bin size as the simulated results so that averaging effects in the direction of the measurement were the same when comparing calculation with measurement.

II.E. Source and geometry tuning procedure

The method used to adjust the source and geometry parameters in the simulation is presented in this section. The simulation geometry is shown in Fig. 1. Secondary collimators (jaws and MLC) were also simulated. The source parameters at the exit window were mean energy, FWHM of the Gaussian peak in the energy distribution, beam angle, FWHM of the Gaussian focal spot, offset of the spot from the collimator rotation axis, and angular distribution. Source and geometry parameters were set by the manufacturer's specification (validated by direct measurement when practical), direct measurement, or through iterative adjustment in the simulation until close matches to measured dose distributions were obtained.

The parameters that were fixed for all beam energies and treatment head configurations were the exit window position, exit window thickness, spot size, primary foil position, secondary foil geometry, secondary collimator positions, and the distance between components (exit window, primary and secondary foil, monitor chamber, and secondary collimators). The energy-dependent parameters, fixed for all treatment head configurations, were the spot position, beam mean energy, peak FWHM and angular distribution FWHM, and primary foil thickness. The geometry parameters changed for different beam energies in the simulation were the secondary foil and monitor chamber offsets from the collimator rotation axis. The beam angle was allowed to change for different beam energies and different treatment head configurations.

The Monte Carlo code used for the simulations did not include an option to simulate a magnetic field. The beam angle and secondary foil and chamber offsets from the collimator rotation axis, even though fixed in reality, were adjusted to accommodate deflection of the electron beam by the magnetic field without directly simulating the field. This means that the simulated beam was not shifted from the initial beam direction, whereas the actual beam was, as seen in Fig. 2. Thus the trajectories of the particles in the simulation were different than the trajectories in the actual beam. Since the electron beam may have been deflected by a different amount for different beam energies, a different shift was used for different beam energies. The monitor chamber shift primarily affected the position of the R_{max} profile edge, the foil shift primarily affected symmetry. The different beam angles used for the different configurations had no impact on the quantities determined for simulation of the clinical configuration.

II.E.1. Spot size and position

The Siemens Oncor and other linac models are equipped with a steering coil. The spot moved inplane when the steering coil current was changed rather than remaining in a fixed position as previously modeled.[6,9] Steering was varied over a wide range for the different beam energies and the shift in spot position determined from the shift in the field edge on the measured R_{max} inplane profile. The spot moved by an amount proportional to the steering current. The change in the spot position per unit current determined from these measurements is shown in Fig. 3. The spot was shifted less at higher energies for the same change in current, as expected.

The spot was simulated as a Gaussian radial distribution of FWHM 0.2 cm offset from the collimator rotation axis by the amount measured from the 5×5 cm^2 R_x scans. The source was at the origin of the coordinate system used in

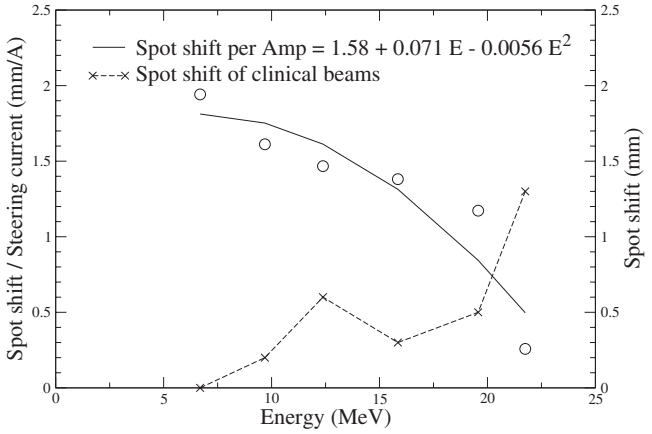

FIG. 3. Shift in the spot position per unit steering current. Each point is from a linear fit to a comprehensive set of measurements of spot shift versus steering current (circles, scale on left side of graph). Also shown is the shift of the clinical beam focal spot when steering current is turned on (dashed line, scale on right side). The energy is kinetic energy of the source used in the simulation.

BEAMnrc, with the source offset from the collimator rotation axis added to the component module shifts. The source offset was accounted for in the dose distributions calculated with MCRTP, with the origin of the simulated and measured dose distributions set to the mechanical isocenter of the linac, on the collimator rotation axis.

II.E.2. Source direction

The direction cosine of the source, both inplane and crossplane, was set to the distance from the focal spot at the exit window to the peak in the profile divided by the distance from the primary foil to the scan depth. The R_{max} profile was used to determine the beam angle for the no foil and primary foil configurations, the R_x profile for the clinical configuration. The collimator setting was 40×40 cm^2. The peak position was determined by fitting a Gaussian to the profile over a limited range where the Gaussian was a reasonable fit to the peak: In the region of the R_{max} profiles where the dose exceeds 50% of the dose on the central axis, out to 10 cm off axis for 6 and 9 MeV R_x profiles, out to 5 cm off axis for higher energies.

A separate set of simulations was done for the clinical beams with the beam angle set to align the beam with the position of the peak in the R_{max} profile in the primary foil configuration. Source and geometry parameters were adjusted iteratively to match the measured dose profiles for the clinical beams. This did not improve the match to the R_{max} profiles as hoped, while the R_x profile peak in the clinical beams were out of place. The approach was dismissed.

II.E.3. Energy distribution

The energy distribution of the source was modeled as a single Gaussian peak. The mean energy was adjusted to match the measured PDI I_{50} in the primary foil configuration. This configuration was chosen, as the depth penetration did not depend on matching the width of the dose distribution as it did for the higher energies in the no foil configuration. The FWHM of the peak in the energy distribution was estimated by matching the slope in the fall-off portion of the PDI curve for both the no foil and primary foil configurations.

II.E.4. Exit window thickness and source divergence

The width of the R_{max} profiles simulated with the exit window as specified by the manufacturer is known to fall 2–3 cm short of measurement.[18] In this separate study, the thickness of the exit window (water and window material) was increased over that specified by the manufacturer to achieve the angular distribution at the downstream surface of the exit window required to match the width of the measured R_{max} profile. The specification is for a channel that is not under pressure. The window could bulge out approximately 0.03 cm, based on the approximate water pressure of 15–20 psi and the Young's modulus of the window material. It was decided to increase the water thickness only and to match the width of the measured R_{max} profile for one of the energies, with the profile width underestimated for the remaining energies. The angular distribution (divergence) of the source for these energies was then increased to match the profile width.

We dismissed several alternatives to explain the underestimate in the profile width. A broader source angular distribution would reduce the required thickness; however, several constraints relegate the angular distribution to a minor source of broadening.[18] Contaminants were not present in the water in sufficient concentration to broaden the beam, shown with measurements done with freshly distilled water in the cooling channel. EGSnrc is proven to be accurate for simulation of electron scatter from foils, for a geometry and energy comparable to the no foil configuration;[4] therefore, the simulation was not at fault.

It would help to have independent verification of the water channel thickness. One possibility considered was to determine the exit window thickness by a measurement of the dose ratio D_x/D_{max} for the no foil configuration. Unfortunately, the change in this ratio with window thickness, assessed with Monte Carlo simulation, turned out to be negligible, as most of the bremsstrahlung in this configuration was from the water.

II.E.5. Primary scattering foil

The primary scattering foil density used was 8.06 g/cm^3 for stainless steel, 19.32 g/cm^3 for gold. Foil thickness was chosen to give a reasonable match to the measured change in the R_{max} profile width from the no foil to the primary foil configuration. Foil thickness varies with position for the gold foils, based on direct measurement with calipers and by steering the beam across the foil and measuring the change in D_x/D_{max}. Therefore, a different foil thickness was allowed for the 18 and 21 MeV beams, which shared the same foil. This is justified as the spot was in a different position for these energies. The dose ratio D_x/D_{max}, used previously to determine the foil thickness,[6,9] was used in this study as

quality control (QC), with the dose at R_x and R_{max} measured on the central axis following the TG-51 protocol.[19]

An alternative method to determine foil thickness is to match the measured shift in the PDI between the no foil and primary foil configuration. In this approach, the width of the R_{max} profile with no foil in place needs to be matched in the simulation for the higher energies to account for the modest dependence of R_{50} on field width. The shift may be measured in a few minutes, reducing uncertainty due to chamber positioning relative to the water surface, water evaporation, etc. It is possible to achieve 0.03 g/cm^2 (5%–20%) accuracy in foil thickness determination with the IBA scanning equipment. Uncertainties include 0.02 cm in the measured shift in I_{50} and 0.02 cm due to uncertainty in the normalization, as the build-up region of the measured and simulated PDIs did not match. This turned out to be not as accurate as the method chosen to determine the foil thickness, relegating the PDI shift method to QC.

II.E.6. Monitor chamber and secondary foil

The monitor chamber distance from the exit window and offset from the collimator rotation axis was adjusted in the simulation to match the field edges of the R_{max} crossplane and inplane profiles in the clinical configuration. The monitor chamber was moved vertically to change the field width and moved horizontally to shift the field edge. Symmetry in the R_{max} profiles was adjusted by moving the secondary foil horizontally.

The retaining ring for the secondary foil did not appreciably cut into the field as the difference between the crossplane and inplane field width for 18–21 MeV was only 0.20 cm. This difference could be due to the magnetic field and the peripheral material below the monitor chamber as well as the retaining ring. The field width was matched to the average of the crossplane and inplane profiles and the retaining ring set outside of the field defined by the monitor chamber. The secondary foil offset from the collimator rotation axis was adjusted to match the symmetry of the R_{max} crossplane and inplane profiles in the clinical configuration.

II.E.7. Secondary collimator positions

The offset of each jaw and the central MLC leaves from the collimator rotation axis was set in the simulation to match the position of the field edge in the R_{max} profiles measured for the higher energy beams in the primary foil configuration. In this configuration, the field was broad enough to be substantially collimated by the secondary collimators, MLC support block, and tray rails. The higher beam energies had the sharpest field edges. The assumption is the effect of the deflection of the electron beam in the stray magnetic field and collimation by the peripheral material downstream of the MLC on the field edge in the clinical configuration can be accommodated by this procedure.

III. SENSITIVITY RESULTS

Source and geometry adjustments were done to match simulated dose distributions to measurement took advantage of a published sensitivity analysis.[14] The results of a limited complementary sensitivity analysis are reported here.

The R_{max} profile width at 50% in the no foil configuration at 6 MeV increased 0.32 cm for a 0.01 cm increase in thickness of the water in the exit window.

Regarding the root-mean-square angle of the source, for the configuration with no foils in the beam and the exit window set to manufacturer specification, the profile width at 50% maximum changed approximately 2 cm/deg, independent of energy. With a thicker exit window the beam was scattered more and the profile width was less sensitive to changes in the divergence of the source. With the exit window thickness set to match the 6 MeV R_{max} profile width with no angular distribution, the profile width changed approximately 0.6 cm/deg for the 9 MeV beam, 1.1 cm/deg for the 12–21 MeV beams, when the angular distribution results in a simulated profile that was a close match to the measured profiles.

The R_{max} profile width at 50% increased with the primary foil thickness by 0.03 cm/μm at 9 MeV, 0.12 cm/μm at 12 MeV, and 0.03 cm/μm at 15–21 MeV.

A thicker foil decreased D_{max}/N_e while increasing D_x/N_e, where N_e is the number of source electrons. These effects increased D_x/D_{max} in the primary foil configuration by 0.4%/μm foil thickness for the 9 MeV beam, 0.8%/μm for the 12 and 15 MeV beams, 0.4%/μm at 18 MeV, and 0.2%/μm at 21 MeV.

A 0.264 cm change in the distance from the exit window to the primary foil changed the off-axis ratio in the R_{max} profile by no more than 0.5% at any energy out to (but not including) the field edge. The result is applied to the three treatment head configurations.

A 0.2 cm increase in the distance from primary foil to secondary foil resulted in a 2% decrease in the off-axis ratio of the R_{max} profile in the clinical beam at 21 MeV. There was reduced sensitivity to a change in the distance between foils with decreasing energy.

The change in I_{50} with source energy was fit to a linear-quadratic function. The quadratic term was needed to account for the narrow profiles of the higher energy beams, leading to a reduced slope in the fall-off region of the PDI. The energies calculated with the fit were within 0.9% of the energies used in the simulation through the full energy range of 6.7–21.7 MeV. The sensitivity of the depth penetration to energy in the no foil configuration, dE/dI_{50} was 1.83 MeV/cm+0.123I_{50} MeV/cm^2. This relationship is not to be confused with published energy-range relationships that refer to the energy at the water surface

The PDI I_{50} change with energy in the primary foil configuration was approximately linear through the full energy range of 9.7–21.7 MeV with dE/dI_{50}=2.57 MeV/cm. A quadratic term was unnecessary as the profiles were broad enough to have I_{50} independent of the profile width. The energy in the fit differed from the data used in the fit by as much as 1.5% since the different primary foils used for each beam led to an energy-dependent shift in the PDI.

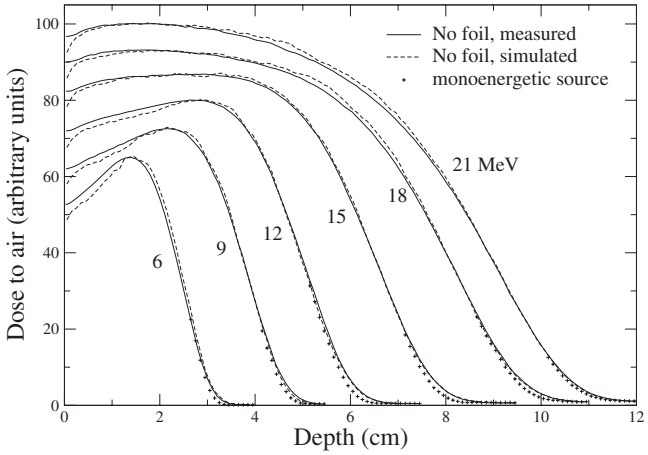

FIG. 4. Depth ionization curves for the no foil configuration measured with a parallel-plate chamber (solid lines). Simulated result with (dashed line) normalized to agree with the measured dose at R_{max} (Table I). Results of simulations with a monoenergetic source at the exit window are also shown (plus signs).

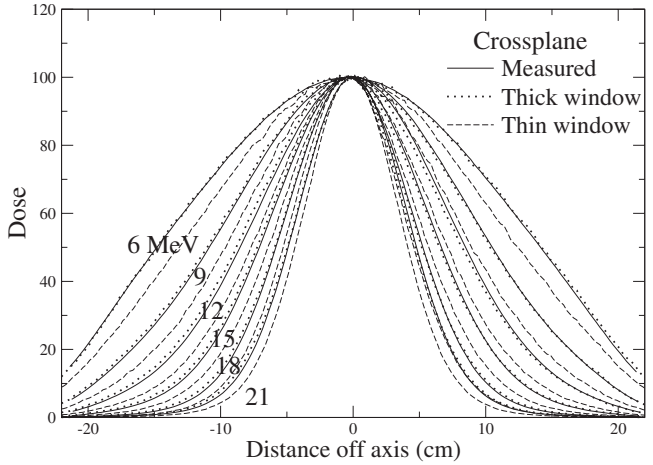

FIG. 5. Crossplane R_{max} profiles for the no foil configuration. Measurement compared to simulation. The "thick window" simulations are with the thickness of water in the exit window increased to match the measured 6 MeV profile. The "thin window" simulations are with the exit window thickness specified by the manufacturer.

IV. RESULTS AND DISCUSSION

IV.A. No foil configuration

The measured and simulated PDIs for the no foil configuration are shown in Fig. 4. The I_{50} agrees to 0.06 cm (Table I), showing that the beam was stable between measurements (the primary foil configuration was used to determine the energy) and that the estimated uncertainty in the measurement of I_{50} was reasonable. The dose from R_{max} to the depth of 80% dose agrees to $1.0 \pm 0.3\%$. The simulated dose in the build-up region from 0.1 cm to R_{max} varies from $3.0 \pm 0.3\%$ lower than measured at 6 MeV to $0.6 \pm 0.3\%$ lower at 21 MeV. The distance to agreement with the measured PDI from the depth of 80% dose to the practical range region is generally 0.06 cm or better. The exception is for the two highest energy beams where the distance to agreement reaches 0.10 cm in the region at the depth of 80% dose.

The simulated and measured R_{max} crossplane profiles are in close agreement, slightly shifted relative to each other (Fig. 5). Inplane results were comparable. The result could be improved by adjusting the beam angle; however, the beam angle was not a critical parameter in this configuration. The important result was the profile width, used to determine the thickness of the exit window and source divergence, and with the profiles measured in the primary foil configuration, to determine the primary foil thickness. The widths of the measured inplane profiles were up to 0.3 cm wider than the crossplane profiles at 50% of the maximum dose (Table III). The average of the inplane and crossplane profile widths was matched to 0.13 cm. The discrepancy at the field edge would be half of this (0.07 cm) if the beam angle were more carefully chosen.

The water channel thickness was increased 0.05 cm over manufacturer specification (Table II) to match the R_{max} profile width on the 6 MeV beam in the no foil configuration (Fig. 5). A source angular distribution with mean angular spread up to 0.4°–0.8° was required for the remaining beams (Table IV).

The crossplane profiles at R_{max} for the no foil configuration shown in Fig. 5 include a set of profiles simulated with the window thickness specified by the manufacturer, with all other source and geometry details the same as in the simulation with the thicker exit window. There is a significant deficit in the angular distribution in this case, demonstrating that the divergence of the beam emerging from the foil is much broader than simulated with the thinner window. In a separate set of simulations the source angular distribution was increased to match the profile width, resulting in a peak in the R_x profile for the clinical beam that was much to broad, with D_x/D_{max} underestimated by 15% on the central axis for the higher energy beams. This approach was abandoned.

IV.B. Primary foil configuration

The measured and simulated PDIs for the primary foil configuration are shown along with those measured in the no foil configuration in Fig. 6. The energy loss in the primary foil shifts the PDI toward the water surface, with a sharper falloff for the higher energy beams, broadened by scattering in the foil. The penetration depth I_{50} obtained from a linear fit in the 40%–60% dose region of the PDIs (Table I) was used to set the beam energy in the simulation (Table IV) with an accuracy of 1.4% at 6 MeV, decreasing to 0.8% at 21 MeV. This includes calculation precision, a 0.5% uncertainty in the stopping power,[11] and a 0.07 cm uncertainty in the measured I_{50}. The maximum difference in I_{50} from the mean for the three sets of primary foil Roos PDIs (average shown in Fig. 6) was 0.04 cm, with the difference strongly correlated with date of measurement (and not with beam energy). This is consistent with the 0.03 cm uncertainty in depth position with minimal drift in beam energy over the 1–2 months of the measurement.

TABLE III. Width of measured IP and CP R_{max} profiles at 50% of profile maximum and offset of profile peak from collimator rotation axis, for no foil and primary foil configurations with jaw and MLC fully open. Offset is position of peak of Gaussian, determined from fit in region of dose greater than 50%. The 6 MeV beam had no primary foil. Width and offset for the clinical beam based on the position of the point that was 50% of the dose measured at the point 15 cm from the collimator rotation axis.

		Nominal beam energy (MeV)					
Configuration	Measurement	6	9	12	15	18	21
No foil measurement	IP Width (cm)	29.03	21.65	17.26	13.99	11.23	9.95
	CP Width (cm)	28.94	21.36	17.02	13.73	11.10	9.69
	IP Offset (cm)	−1.16	−1.14	−1.00	−0.99	−0.87	−1.16
	CP Offset (cm)	−0.34	−0.18	−0.03	−0.21	−0.28	−0.06
No foil simulation	IP Width (cm)	28.84	21.48	17.01	13.76	11.21	9.73
	CP Width (cm)	28.94	21.35	17.02	13.78	11.09	9.67
	IP Offset (cm)	−1.22	−1.20	−1.27	−1.10	−0.88	−1.25
	CP Offset (cm)	−0.35	−0.32	−0.32	−0.36	−0.36	−0.14
Primary foil measurement	IP Width (cm)	No foil	32.10	31.07	37.10	35.90	33.19
	CP Width (cm)	No foil	31.96	30.60	37.03	35.71	32.66
	IP Offset (cm)	No foil	−1.15	−1.24	−1.24	−1.01	−1.50
	CP Offset (cm)	No foil	−0.21	0.15	0.32	0.32	0.65
Primary foil simulation	IP Width (cm)	No foil	31.77	30.78	37.01	35.65	33.03
	CP Width (cm)	No foil	31.83	30.49	37.19	35.76	32.94
	IP Offset (cm)	No foil	−1.15	−1.33	−1.24	−1.09	−1.54
	CP Offset (cm)	No foil	−0.22	0.17	0.27	0.26	0.68
Clinical beam measurement	IP Width (cm)	40.16	39.80	39.24	38.90	37.26	35.96
	CP Width (cm)	40.41	39.87	38.23	38.82	37.15	35.96
	IP Offset (cm)	−0.71	−0.81	−1.14	−0.93	−1.08	−1.99
	CP Offset (cm)	−0.28	−0.08	0.20	0.38	0.33	0.48

The energy varied linearly with bending magnet current up to 19.6 MeV, a reliable QC of the energies used in the simulation. The least-squares linear fit, leaving out the 21.75 MeV point, had an intercept of −0.53 MeV and slope of 0.546 MeV/A and was within 1.4% of the simulated energy for the nominal 6 MeV beam, the fit improving with increasing energy to 0.6% for the nominal 18 MeV beam, within experimental uncertainty. The magnet showed signs of saturation at 13.4 A, corresponding to an energy of 21.75 MeV.

The FWHM of the Gaussian energy distribution, chosen to match the falloff of the measured PDI, is listed in Table IV. The broadening of the energy distribution mainly affected the toe of the distribution (Fig. 4). An estimated 0.03 cm uncertainty in the measured position of the toe region relative to I_{50} leads to a 30% uncertainty in the FWHM.

The measured and simulated R_{max} crossplane profiles for the primary foil configuration are compared in Fig. 7. Inplane results were comparable. The jaws and MLC positions used in the simulation (Table II) resulted in a close match to the profile edge. The profile widths are 0.1–0.6 cm larger inplane than crossplane, carried over from the no foil configuration. The primary foil thicknesses used in the simula-

TABLE IV. Energy-dependent source parameters at the exit window used in the simulation for all configurations unless otherwise stated. Mean energy was the same for Gaussian and Parmela spectra. Parmela spectrum FWHM from Gaussian fit. Root mean square angular divergence. Spot position relative to the collimator rotation axis. Direction cosine used for the clinical configuration.

		Nominal beam energy (MeV)					
		6	9	12	15	18	21
Mean energy (MeV)		6.69	9.69	12.38	15.85	19.57	21.75
FWHM (MeV)	Gaussian	0.94	0.94	1.53	1.88	1.88	1.41
	Parmela	0.72	0.91	0.91	0.58	0.92	1.75
Angular divergence (deg)		0	0.8	0.55	0.8	0.75	0.4
Spot Position	Crossplane (cm)	−0.05	−0.03	−0.03	−0.03	−0.02	−0.02
	Inplane (cm)	0	0.02	0.07	0.04	0.04	0.18
Direction cosine	Crossplane (cm)	−0.002	−0.004	0.001	0.002	0.003	0.005
	Inplane (cm)	0	0	−0.002	0	0.002	−0.003

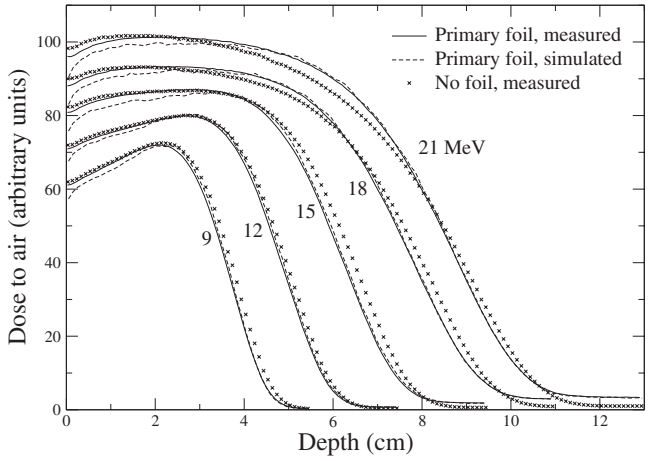

FIG. 6. Depth ionization curves for the primary foil configuration measured with a parallel-plate chamber (solid lines). Measurements compared to Monte Carlo simulation (dashed lines) using the same beam energy and spectral width as the no foil case. The no foil measurements are also shown (crosses).

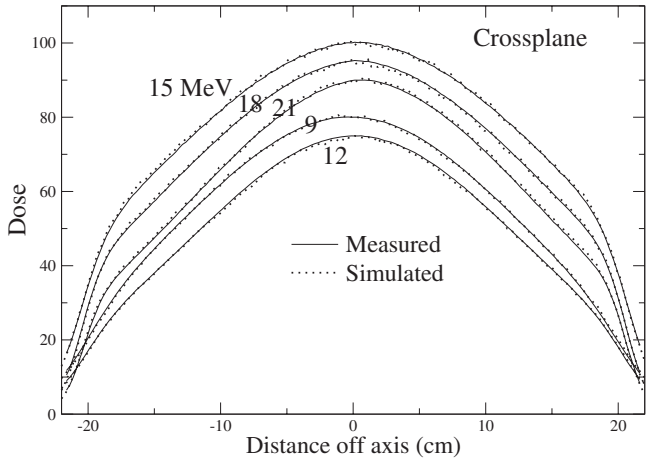

FIG. 7. Crossplane R_{max} profiles for the primary foil configuration.

tion resulted in a match to the measured profile half-widths, averaged inplane and crossplane, of 0.12 cm or better (Table III).

The primary foil thickness used in the simulation (Table II) agrees within 2 standard deviations of manufacturer specification for the 9–15 MeV foils, and is 5 standard deviations out for the 18 and 21 MeV foils. The uncertainty was 6% at 9–12 MeV and 1% at 15–21 MeV. The deviations from specification are realistic, as the gold foil thickness is known to vary across the foil. The calculated shift in the PDI curves between the no foil and primary foil configuration agrees with measurement to within 0.03 ± 0.03 cm for all six beam energies, an approximate QC on foil thickness.

The ratio of the charge collected by the parallel-plate chamber at R_x and R_{max}, Q_x/Q_{max}, was much easier to measure than D_x/D_{max}. The D_x/D_{max} method appears to slightly overestimate primary foil thickness and should be used with caution. The results for the Roos chamber (Table V) show that the measured value of D_x/D_{max} equals $1.100 Q_x/Q_{max}$ to within 1.2% for the 9–21 MeV clinical beams. This result could be used to check the measured dose ratio without performing the more difficult protocol calibration.

There was a notable shift in the position of the profile peak of up to 0.7 cm in the crossplane direction when changing from the no foil configuration to the primary foil configuration, with the shift increasing with energy (Table III). The reason for this was not determined.

IV.C. Clinical configuration

The simulated dose distributions on the central axis (Fig. 8) and at R_{max} and R_x (Fig. 9), plotted with the ratio D_x/D_{max} (Table V) preserved, are in better agreement with measurement than the previously published result.[6] The results are for a different machine with the same model of treatment head and the same nominal beam energies. The 15 MeV beam was scattered by a thinner primary foil than the 18 and 21 MeV beam, whereas the same foil was used in the previous study.

The rapid buildup of the simulation matches the diode PDD in the first millimeter. The parallel-plate chamber wall is too thick (0.01 cm) to measure the rapid buildup. Ignoring the first millimeter, the 6 MeV result measured with both types of detectors agrees within 1.0% dose difference (with D_{max} set to 100%) for the full depth range, 1.5% for the 6 MeV beam. The diode over-response in the bremsstrahlung tail is evident.

TABLE V. Dose at R_x relative to dose at R_{max} on the collimator rotation axis, D_x/D_{max}, for the clinical configuration. Measured and simulated results, the latter with precision of calculation for last digit, 1 standard deviation, in brackets. The ratio is the simulated result divided by measurement. Charge collected with Roos chamber at R_x at profile peak relative to the charge collected at R_{max}, Q_x/Q_{max}, ratio is measured $(Q_x/Q_{max})/(D_x/D_{max})$.

Nominal beam energy (MeV)	Depth (cm)		D_x/D_{max}			D_x/D_{max} 0–25 cm Ratio		Q_x/Q_{max}	
	R_{max}	R_x	Measured	Simulated	Ratio	Inplane	Crossplane	Roos	Ratio
6	1.3	6	0.003 42	0.003 35(5)	0.980	0.974	0.975	0.002 84	0.830
9	2.0	7	0.008 14	0.007 47(13)	0.918	0.910	0.927	0.007 31	0.898
12	2.7	8	0.0134	0.0127(1)	0.948	0.946	0.960	0.0122	0.910
15	3.0	10	0.0323	0.0302(2)	0.935	0.978	0.963	0.0296	0.916
18	2.1	12	0.0439	0.0420(2)	0.957	0.996	0.992	0.0401	0.913
21	1.9	13	0.0478	0.0456(2)	0.954	0.950	0.960	0.0434	0.908

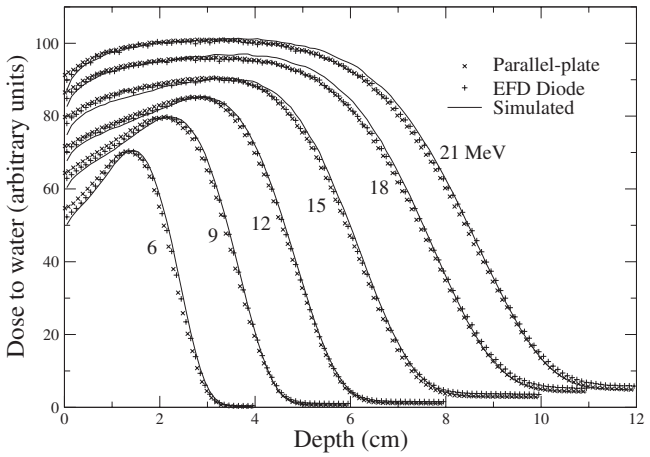

FIG. 8. Depth dose curves in the clinical configuration, measured with a Roos parallel-plate chamber (crosses) and EFD diode (plus signs), compared to the simulated result (solid lines). The curves are normalized at the R_{max} listed in Table I.

The simulated I_{50} is 0.09 ± 0.08 cm deeper than the parallel-plate chamber result, the simulated R_{50} 0.09 ± 0.05 cm shallower than the diode result (Table I). This confirms the choice of the mean energy used in the simulation, from measurements made in the no foil and primary foil configurations. The dose measured with both the parallel-plate chamber and diode builds up more slowly than the simulated PDDs, as observed in the no foil and primary foil configurations. This discrepancy has been reported previously for a parallel-plate chamber[6] and diode.[20] An unrealistic intermediate energy peak would improve the match to measurement, whereas a broader peak in the energy distribution would not. The discrepancy may be due to a change with depth in the charge collected by the Roos chamber per unit dose to water, as discussed earlier, or to an error in the simulation. An accurate PDD measured on a research linac with accurately known energy and beam line components, such as available at NRCC, would help clarify whether the discrepancy exists and help determine the root cause.

Parmela[21] was used to calculate the source energy distributions used in the previous study. This has the drawback that the code requires information on the accelerator that is not generally available. In addition, the spectra calculated with Parmela did not provide as good a match to the measured PDDs as a simple Gaussian peak as follows. The full set of beams was simulated in the clinical configuration with the Gaussian spectra replaced with the Parmela spectra from the previous study, shifted to the mean energy in Table IV, to

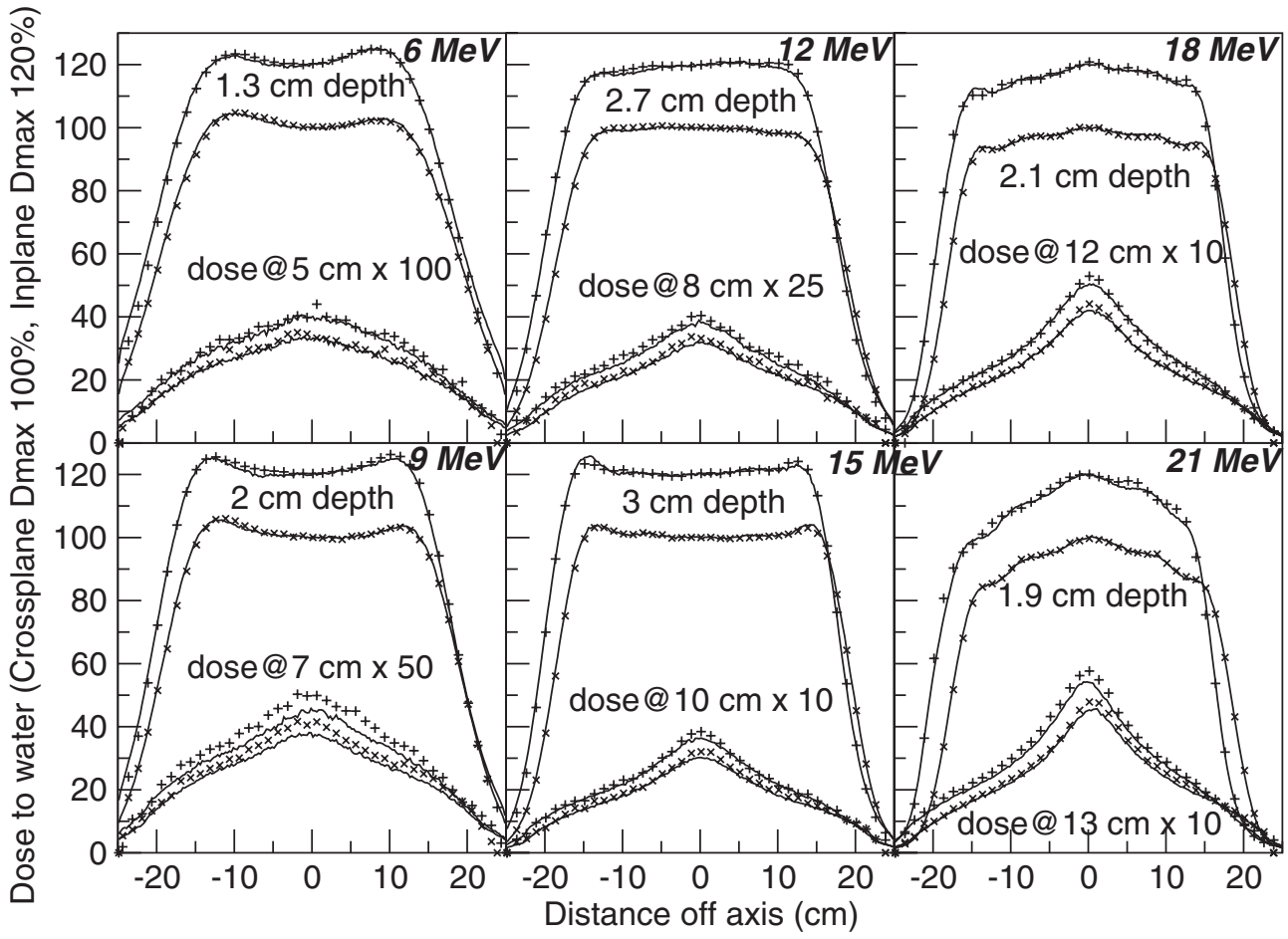

FIG. 9. Inplane and crossplane R_{max} and R_x profiles in the clinical configuration, comparing ion chamber measurement (points) to simulation (lines). Only one out of every five points in the measured profiles is shown for clarity.

give the depth penetration measured for the current study. The simulated PDDs with Parmela spectra fell short at the toe for the 6 and 12–18 MeV beams, intermediate between the measured PDI and those simulated with the monoenergetic spectra (Fig. 4) due to an underestimate of the peak width (Table IV). More detailed information on the spectra may be needed for some applications such as simulation of leakage from x-ray targets[22] and in these cases a code like Parmela may prove helpful.

Simulated and measured profiles are compared in Fig. 9. The larger inplane profile width measured in the no foil and primary foil configurations is not evident for the clinical beams, suggesting an asymmetric source angular distribution would not improve the accuracy of the clinical beam simulation. The origin of the measured profiles, on the collimator rotation axis, was found within 0.02 cm. The alternative used previously of centering the detector on an x-ray field could result in a 0.1–0.2 cm shift in the origin from the collimator rotation axis for calibrated collimators. The spot was previously positioned directly above the scan origin, resulting in a further error in the spot position.

The offset of the monitor chamber from the collimator rotation axis (Table II) reasonably accounts for the shift in the field edge due to the deflection of the beam from the stray magnetic field. The offset of the scattering foil (Table II) results in a reasonable match of beam symmetry. However, the positions of the inflection points in the measured profiles for the higher energy beams are not matched. These are due to the steps in the secondary foil, offset slightly in the simulation from their actual position. Different offsets were needed to account for the magnetic field at different beam energies. The range in foil offset was 0.09 cm crossplane and 0.15 cm inplane. The range in monitor chamber offset was 0.14 cm crossplane and 0.07 cm inplane.

The secondary foil offset from the collimator rotation axis may be better determined with a measurement with the monitor chamber out of the beam. This would also be helpful in determining the position of the ring used to retain the secondary foil, as the ring may intrude into the beam when the monitor chamber is in place. If this were done, the procedure would be to use scans with the monitor chamber in place to get the distance of the monitor chamber and secondary scattering foil from the primary scattering foil, matching R_{max} profile field edges. The monitor chamber would then be removed and scans taken with the secondary foil in position to get the correct offset for the secondary foil.

The beam angle was set by measurement, removing a tunable parameter from the simulation, used previously to adjust symmetry of the R_{max} profile. It turned out to be unnecessary to adjust the beam angle for this purpose, as the R_{max} profile symmetry was matched effectively by moving the secondary scattering foil.

Dose differences of the R_{max} profiles are shown in Fig. 10. The results are a significant improvement over the previous study where the discrepancy was as high as 5.9% at doses of 80% and over, 5.3% out to 12.5 cm, with the largest discrepancy at the edge of the 15 MeV beam for that study. The secondary foil geometry and density were measured directly,

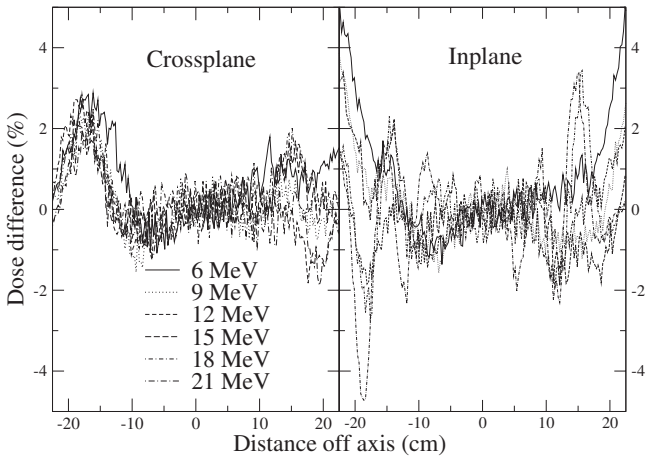

FIG. 10. Difference in R_{max} profiles in the clinical configuration, simulated dose less measured dose, with profiles normalized to 100% in a small region about the central axis prior to subtraction.

confirming manufacturer specification. The excellent match of the flatness of the R_{max} profiles in the clinical beam, with the secondary foil in the beam, demonstrates this geometry and density works effectively in the simulation.

The measured and simulated profiles at the edge of the field are compared in Figs. 11 and 12. The crossplane field edges matched to within 0.16 cm or better. However, the extreme position of the inplane field edges were overestimated by 1.4 cm in the 6 MeV clinical beam simulation, 0.5 cm for 9 MeV, 0.4 cm for 12 MeV, 0.3 cm for 15 MeV, and 0.1 cm for 18–21 MeV. The track for the outer MLC leaves and the rails used to support the accessory trays were added in a separate set of simulations, demonstrating the bulk of the discrepancy would be removed by including these peripheral components in the simulation. Profiles measured at R_{max} without the rails closely matched those measured with the rails, showing that it is unnecessary to include the rails in the simulation. The magnetic field could also contribute to the discrepancy.

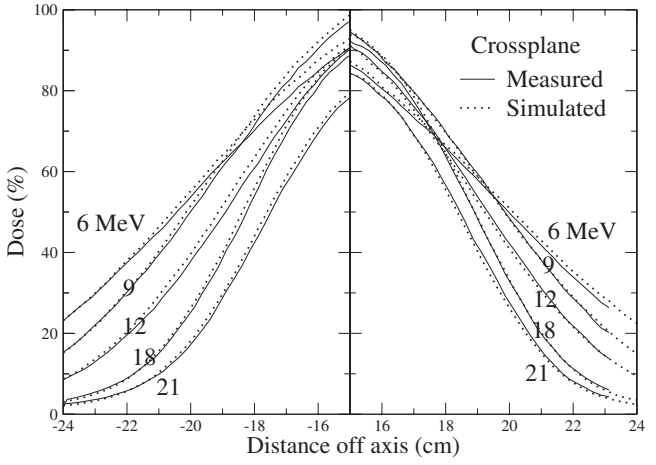

FIG. 11. Crossplane R_{max} profiles at the edge of field in the clinical configuration. Profiles normalized to 100% in a small region about the central axis.

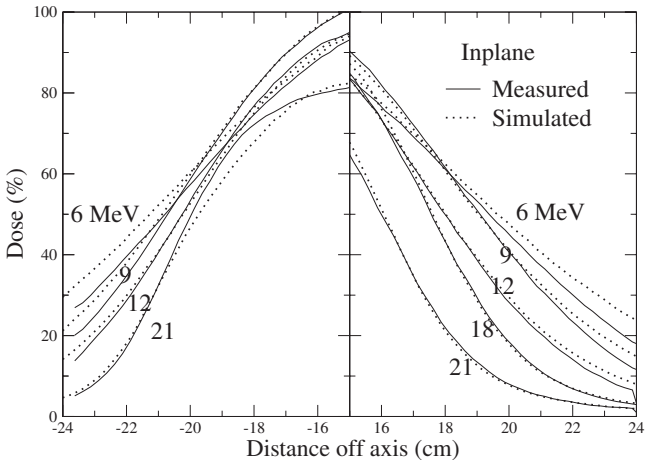

FIG. 12. Inplane R_{max} profiles at the field edge in the clinical configuration. Profiles normalized to 100% in a small region about the central axis.

The peaks in the measured and simulated R_x profiles coincide since the beam angle was chosen for this purpose (Fig. 9). The dose ratio D_x/D_{max} was underestimated in the simulation (Table V). The underestimate for the higher beam energies where the dose ratio is the highest (12–21 MeV) was an average $3 \pm 3\%$ in the region out to 25 cm from the beam axis. The result is within the 5% accuracy of the experimental benchmark of thick-target bremsstrahlung production.[8] Without a more accurate benchmark of dose per source electron in x ray and electron fields, the dose ratio in the simulations was considered acceptable.

IV.D. Alternatives to disassembly

It is possible that, without disassembly of the treatment head, the source and geometry details of a linac similar in model to the Oncor could be determined with accuracy comparable to that achieved here. This would make the method more amenable for clinical machines that have already been commissioned.

The validation of manufacturer specification would apply to components with the same specification. It has already been established that there is a magnetic field that causes significant deflection of the electron beam away for the x-ray beam generated in the exit window and primary scattering foil and that this deflection can be accommodated with energy-dependent offsets of the foil and monitor chamber from the collimator axis. The exit window thickness, source divergence, spot position, mean energy and FWHM of the energy distribution, and thickness of the primary scattering foil could be determined from the change in field flatness observed when the primary foil is removed from the beam, without disassembly. The accuracy of the source and geometry parameters determined from these measurements may suffer from the presence of the secondary foil and monitor chamber. However, direct measurement has verified the geometry and density of the secondary foil, which should not be varied from manufacturer specification in the simulation. The position of secondary collimators could be established from scans of the x-ray beams used for treatment.

V. CONCLUSIONS

A refined method presented for Monte Carlo simulation of large electron fields resulted in tighter constraints on source and geometry details and higher accuracy in the simulated dose distributions. The spot size and position were measured independently. Dose distributions were measured with only the exit window in the beam path, with the primary foil inserted and in the configuration used for treatment, with scattering foils and monitor chamber in place. More care was taken with detector positioning, with the origin set on the collimator rotation axis, and comparison done to depth dose curves measured in a water tank with 0.01 cm positioning precision. An ionization chamber used for R_{max} profile scans improved accuracy over the diode measurements.

Manufacturer specification was verified by direct measurement in many cases, facilitated by disassembly of the treatment head. Changes from specification outside of a reasonable tolerance were justified. The cooling channel of the exit window was thicker than specified, due to water pressure causing the window to bulge out. The gold foil's thicknesses were significantly different than specification, as in the previous study, consistent with the measured variation in thickness across the foils. Vertical and horizontal component shifts away from specification were within our own experience of the tolerance, except for the secondary foil and monitor chamber shifts. The offsets of the secondary scattering foil and monitor chamber from the collimator rotation axis, allowed to vary with energy, accounted for the effect of the deflection of the electron beam by the magnetic field without direct simulation of the field. This would require mapping of the field, a difficult measurement for a linac in a clinical setting.

It is hoped that the revised procedure will make it much easier for others to achieve comparable accuracy in large field simulation for their clinical linac. Certain results are applicable to other linacs of the same model, such as the verification of manufacturer specification of critical components. The removal of the monitor chamber and scattering foil is accomplished easily and in our experience these components can be placed back in the treatment head and the positions adjusted in under a day to reasonably reproduce the original dose distributions. Further work may show that comparable results can be achieved without linac disassembly.

Accuracy might be improved by including the magnetic field in the simulation. In this case, the offset of the secondary foil and monitor chamber from the collimator rotation axis could be fixed in the simulation, independent of the beam energy. If the difference in the inplane and crossplane profile width is not matched in the no foil and primary foil configurations when the magnetic field is added, then an asymmetric angular distribution could be used.

Accuracy might also be improved with the availability of additional experimental benchmarks of Monte Carlo codes to sort out the remaining discrepancies between Monte Carlo simulation with the different codes, the existing experimental benchmarks, and the clinical beam measurements. Desired benchmarks include in-air profiles in electron beams in the

5–10 MeV energy range and x-ray beams in the 5–25 MeV energy range, both with 1% accuracy in fluence in the region where fluence drops to 50% of the maximum. Another useful benchmark is dose per source electron at the depth of maximum dose and in the bremsstrahlung tail, D_{max}/N_e and D_x/N_e. Exacting measurements of dose profiles and PDDs in the benchmark geometries would help bridge the existing experimental benchmarks and the clinical beam results.

The phase-space data used to calculate the dose distributions are, to our knowledge, the most accurate and detailed calculated to date for large electron fields. Fluence distributions calculated from the phase-space files are useful for benchmarking beam models and for other applications in radiotherapy. The phase-space files have been uploaded to the IAEA phase-space data depository on the web to make them generally available at http://www-nds.iaea.org/phsp.

ACKNOWLEDGMENTS

The authors appreciate the work done by Jianwei Chen to measure the spot shift with bending magnet current, the assistance of Val Taranenko for measurement and modification of BEAMnrc, and the comments that James Satterthwaite provided on the manuscript. This work was supported by the U.S. National Institutes of Health under Grant No. R01 CA104777.

[a]Electronic mail: bfaddegon@radonc.ucsf.edu

[1]C. M. Ma, M. Ding, J. S. Li, M. C. Lee, T. Pawlicki, and J. Deng, "A comparative dosimetric study on tangential photon beams, intensity-modulated radiation therapy (IMRT) and modulated electron radiotherapy (MERT) for breast cancer treatment," Phys. Med. Biol. **48**, 909–924 (2003).

[2]E. E. Klein, M. Mamalui-Hunter, and D. A. Low, "Delivery of modulated electron beams with conventional photon multi-leaf collimators," Phys. Med. Biol. **54**, 327–339 (2009).

[3]I. J. Chetty, B. Curran, J. E. Cygler, J. J. DeMarco, G. Ezzell, B. A. Faddegon, I. Kawrakow, P. J. Keall, H. Liu, C. Ma, D. W. O. Rogers, J. Seuntjens, D. Sheikh-Bagheri, and J. V. Siebers, "Report of the AAPM Task Group No. 105: Issues associated with clinical implementation of Monte Carlo-based photon and electron external beam treatment planning," Med. Phys. **34**, 4818–4853 (2007).

[4]C. Ross, M. McEwen, A. McDonald, C. Cojocaru, and B. Faddegon, "Measurement of multiple scattering of 13 and 20 MeV electrons by thin foils," Med. Phys. **35**, 4121–4131 (2008).

[5]C.-M. Ma and S. B. Jiang, "Monte Carlo modelling of electron beams from medical accelerators," Phys. Med. Biol. **44**, R157–R189 (1999).

[6]B. A. Faddegon, B. Perl, and M. Asai, "Monte Carlo simulation of large electron fields," Phys. Med. Biol. **53**, 1497–1510 (2008).

[7]R. Weinberg, J. A. Antolak, G. Starkschall, R. J. Kudchadker, R. A. White, and K. R. Hogstrom, "Influence of source parameters on large-field electron beam profiles calculated using Monte Carlo methods," Phys. Med. Biol. **54**, 105–116 (2009).

[8]B. A. Faddegon, M. Asai, J. Perl, C. Ross, J. Sempau, J. Tinslay, and F. Salvat, "Benchmarking of Monte Carlo simulation of bremsstrahlung from thick targets at radiotherapy energies," Med. Phys. **35**, 4308–4317 (2008).

[9]B. A. Faddegon, E. Schreiber, and X. Ding, "Monte Carlo simulation of large electron fields," Phys. Med. Biol. **50**, 741–753 (2005).

[10]I. J. Das, C.-W. Cheng, R. J. Watts, A. Ahnesjö, J. Gibbons, X. Allen Li, J. Lowenstein, R. K. Mitra, W. E. Simon, and T. C. Zhu, "Accelerator beam data commissioning equipment and procedures: Report of the TG-106 of the Therapy Physics Committee of the AAPM," Med. Phys. **35**, 4186–4215 (2008).

[11]International Commission on Radiation Units and Measurements, "Stopping powers for electrons and positrons," ICRU Report No. 37, 1984.

[12]D. X. Ding, D. W. O. Rogers, and T. R. Mackie, "Calculation of stopping-power ratios using realistic clinical electron beams," Med. Phys. **22**, 489–501 (1995).

[13]E. Chin, H. Palmans, D. Shipley, M. Bailey, and F. Verhaegen, "Analysis of dose perturbation factors of a NACP-02 ionization chamber in clinical electron beams," Phys. Med. Biol. **54**, 307–326 (2009).

[14]E. Schreiber and B. A. Faddegon, "Sensitivity of large-field electron beams to variations in a Monte Carlo accelerator model," Phys. Med. Biol. **50**, 769–778 (2005).

[15]D. W. O. Rogers, B. A. Faddegon, G. X. Ding, C.-M. Ma, J. We, and T. R. Mackie, "BEAM: A Monte Carlo code to simulate radiotherapy treatment units," Med. Phys. **22**, 503–524 (1995).

[16]I. Kawrakow, "Accurate condensed history Monte Carlo simulation of electron transport. I. EGSnrc, the new EGS4 version," Med. Phys. **27**, 485–498 (2000).

[17]B. A. Faddegon, J. Balogh, R. Mackenzie, and D. Scora, "Clinical considerations of Monte Carlo for electron radiotherapy treatment planning," Radiat. Phys. Chem. **53**, 217–227 (1998).

[18]D. Sawkey and B. Faddegon, "Determination of electron source parameters at the exit window for clinical megavoltage x-ray beams," Med. Phys. **36**, 698–707 (2009).

[19]P. R. Almond, P. J. Biggs, B. M. Coursey, W. F. Hanson, M. S. Huq, R. Nath, and D. W. O. Rogers, "AAPM's TG-51 protocol for clinical reference dosimetry of high-energy photon and electron beams," Med. Phys. **26**, 1847–1870 (1999).

[20]K. R. Shortt, C. K. Ross, A. F. Bielajew, and D. W. O. Rogers, "Electron beam dose distributions near standard inhomogeneities," Phys. Med. Biol. **31**, 235–249 (1986).

[21]L. M. Young, "PARMELA user manual," Los Alamos National Laboratory Report No. LA-UR-96-1835, 2003.

[22]B. Faddegon, V. Wu, J. Pouliot, B. Gangadharan, and A. Bani-Hashemi, "Low dose megavoltage cone beam CT with an unflattened 4 MV beam from a carbon target," Med. Phys. **35**, 5777–5786 (2008).